PAPER

Coupling of photonic crystal cavity and interlayer exciton in heterobilayer of transition metal dichalcogenides

2D Materials

PAPER

Coupling of photonic crystal cavity and interlayer exciton in heterobilayer of transition metal dichalcogenides

RECEIVED
9 September 2019

REVISED
29 October 2019

ACCEPTED FOR PUBLICATION
20 November 2019

PUBLISHED
11 December 2019

Pasqual Rivera[1], Taylor K Fryett[2], Yueyang Chen[2], Chang-Hua Liu[1,3], Essance Ray[1,4], Fariba Hatami[5], Jiaqiang Yan[6,7], David Mandrus[6,7,8], Wang Yao[9], Arka Majumdar[1,2,10] and Xiaodong Xu[1,4,10]

[1] Department of Physics, University of Washington, Seattle, Washington, United States of America
[2] Department of Electrical and Computer Engineering, University of Washington, Seattle, Washington, United States of America
[3] Institute of Photonics Technologies, National Tsing Hua University, Hsinchu 30013, Taiwan
[4] Department of Materials Science and Engineering, University of Washington, Seattle, Washington, United States of America
[5] Department of Physics, Humboldt University, D-12489 Berlin, Germany
[6] Materials Science and Technology Division, Oak Ridge National Laboratory, Oak Ridge, Tennessee, United States of America
[7] Department of Materials Science and Engineering, University of Tennessee, Knoxville, Tennessee, United States of America
[8] Department of Physics and Astronomy, University of Tennessee, Knoxville, Tennessee, United States of America
[9] Department of Physics and Center of Theoretical and Computational Physics, University of Hong Kong, Hong Kong, People's Republic of China
[10] Author to whom any correspondence should be addressed.

E-mail: xuxd@uw.edu **and** arka@uw.edu

Keywords: nanoresonator, interlayer exciton, cavity quantum electrodynamics

Supplementary material for this article is available online

Abstract

The advent of van der Waals heterostructures marks the emergence of a new class of synthetic materials with novel properties that are unattainable in their constituent materials. The 2D architecture of these layered materials makes them naturally suited for integration with a wide variety of planar nanophotonic cavities for next-generation low-power optoelectronic devices and explorations of fundamental physical effects in these new systems. Here, we report the coupling of the interlayer exciton in a transition metal dichalcogenide heterobilayer with a gallium phosphide photonic crystal defect cavity. The exciton-cavity coupling is found to be in the weak regime, resulting in ~15-fold increase in the photoluminescence intensity for interlayer exciton in resonance with the cavity. Simulation results suggest that the increased intensity stems from a Purcell enhancement of ~60. The order of magnitude enhancement of the photoluminescence yield offsets the low oscillator strength of the interlayer exciton, adding a new tool for probing the underlying physics of this excitonic system.

The recent advances in fabrication and characterization of two-dimensional (2D) materials and heterostructures present new opportunities for engineering ultrathin synthetic quantum materials with unique physical properties [1, 2]. Among the many recently developed heterostructures, heterobilayers comprised of different monolayer transition metal dichalcogenides (TMDs) have attracted intense research efforts [3]. These composite materials host an atomically sharp type-II electronic interface [4, 5] (figure 1(A)), which results in the formation of an interlayer exciton (IX) [6, 7]—the Coulomb bound state composed of electron and hole localized in different layers (figure 1(B)). This system has emerged as a promising platform for optoelectronic devices with valleytronic functionality [8] and for explorations of the fundamental physics of excitons [3].

The interlayer exciton is the lowest lying optical excitation in TMD heterobilayers, and the spatial separation of the constituent charges results in a number of advantageous properties. In particular, the IX exhibits enhanced exciton population [6, 9] and valley lifetimes [10–12], compared to its monolayer TMD counterparts. Moreover, the intrinsic electric dipole moment of the IX allows for modulation of the exciton energy [6, 13], as well as control of exciton flux [14] by patterned electrodes and gates. However, theoretical [15, 16] and experimental [17] works have revealed small optical dipole moment for IX, with oscillator strength

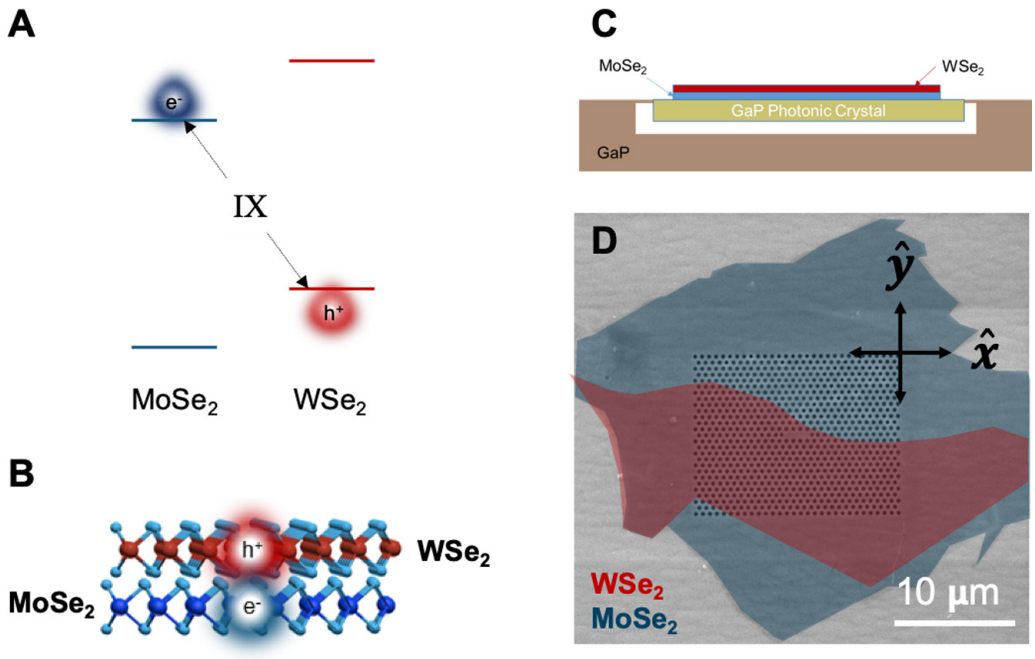

Figure 1. $MoSe_2$–WSe_2 heterobilayer integrated with photonic crystal. (A) Band alignment of the $MoSe_2$–WSe_2 heterobilayer with the interlayer exciton (IX) shown by dashed lines. (B) Side-view illustration of the spatially indirect IX, with electron and hole localized in different layers of the $MoSe_2$–WSe_2 heterobilayer. (C) Side-view of the heterobilayer placed on top of the GaP photonic crystal. (D) Scanning electron micrograph of the $MoSe_2$–WSe_2 heterobilayer on the photonic crytal. The monolayer of WSe_2 is overlaid in red, while the monolayer $MoSe_2$ in blue. The coordinate system is defined by the axis of the linear three-hole defect.

about 2 orders of magnitude lower than that of a single monolayer TMD. This limitation has made optical studies of the IX properties challenging.

On the other hand, the high sensitivity of 2D materials to their dielectric environment makes them suitable for coupling to planar photonic devices. This presents an opportunity to not only overcome the weak optical emission, but also new scientific opportunities, such as exploring exciton-polaritons with valley degrees of freedom at room temperature. Already, monolayer TMDs embedded within distributed Bragg reflector microcavities have demonstrated the formation of valley exciton-polaritons [18, 19]. Moreover, the surface coupling of monolayer TMDs with photonic crystal nano-cavities has given rise to ultra-low threshold nanoscale lasers [24], cavity enhanced light emitting diodes [20], and enhanced second harmonic generation [21–23]. Here, we show that the placement of the TMD heterobilayer on top of a gallium phosphide photonic crystal (PhC) linear three-hole defect cavity results in IX-cavity coupling in the weak regime, with a significant enhancement of the photoluminescence (PL) resulting from the Purcell enhancement of the IX in resonance with the PhC cavity modes.

Results

The sample in our study consists of a $MoSe_2$–WSe_2 heterobilayer placed on top of a gallium phosphide (GaP) linear three-hole defect (L3) photonic crystal cavity, as illustrated in figure 1(C). Photonic crystal cavity is chosen because of the small mode-volume and high-quality factor of the cavities, which give rise to a strong light–matter interaction. The L3 cavity was fabricated by defining an etch-mask on top of a 125 nm GaP thin film on sacrificial layer of InGaP substrate, using electron beam lithography, followed by reactive ion etching, and subsequent removal of the sacrificial layer, as described in our previous work [24]. The photonic crystal cavity was first characterized by cross-polarized reflectivity measurements [25] at 300 K, prior to fabrication and transfer of the heterobilayer. The monolayers of $MoSe_2$ and WSe_2 were mechanically exfoliated from bulk materials and assembled into the heterobilayer using top-down viscoelastic stamping techniques [26]. The straight edges of the monolayer flakes of WSe_2 and $MoSe_2$ were carefully aligned during the fabrication, and the final transfer was directed onto the photonic crystal cavity. We note that aligning the edges is a common technique to achieve samples that are bright, which requires a small twist angle, since the cleaved monolayer WSe_2 and $MoSe_2$ crystals favor zig-zag edges. The brightness of the sample is a reliable indicator that the sample is aligned within about 5°, as we have experienced before in experiments. A scanning electron micrograph of the completed device is shown in figure 1(D), with the different layers of the heterobilayer highlighted in false color for clarity. For further details on the sample fabrication, see methods.

Cross-polarized reflectivity measurements of the bare cavity revealed resonances at $\hbar\omega_1 = 1.37$ eV and $\hbar\omega_2 = 1.33$ eV, with quality factors of $Q_1 = 1370 \pm 140$ and $Q_2 = 780 \pm 50$, respectively (figure S1). The quality factors are estimated by

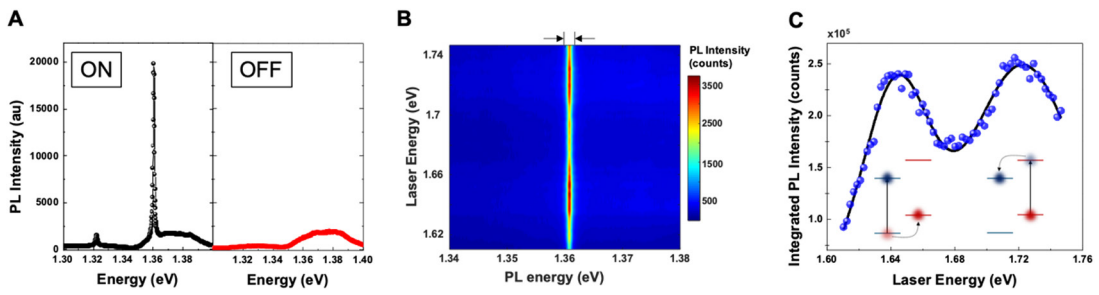

Figure 2. Cavity coupling of the interlayer exciton. (A) Photoluminescence (PL) spectra from on (left) and off (right) the linear three-hole defect cavity in the photonic crystal (PhC). The sharp PL peak present on the cavity is spectrally degenerate with the cavity mode (see figure S1 (stacks.iop.org/TDM/7/015027/mmedia)). (B) Photoluminescence excitation response from the $MoSe_2$–WSe_2 heterobilayer ON the PhC cavity. (C) Integrated PL intensity of the sharp peak in the PL spectrum on the cavity as a function of the excitation laser energy. The black arrows in (B) denote the integration region. Insets: illustration of the formation process of interlayer exciton by photon absorption (solid vertical arrows) in monolayer $MoSe_2$ (left) and monolayer WSe_2 (right), followed by interlayer charge transfer (dashed arrows). This gives rise to the two Gaussian peaks in the PLE response of the interlayer exciton (fit to the data shown in solid black lines).

fitting a single Lorentzian function to the peaks observed in the cavity transmission spectrum. This particular cavity was chosen because the higher energy resonance is well-matched to the PL energy of IX in the $MoSe_2$–WSe_2 heterobilayer [3]. The optical response of the TMD heterobilayer on the PhC was then characterized using confocal PL spectroscopy in reflection geometry, normal to the plane of the heterobilayer, at a temperature of 5 K. A continuous wave (cw) laser ($\lambda = 532$ nm) was used to excite the sample. The PL spectrum of the heterobilayer consists of emission from intralayer excitons in the energy region of ~1.6–1.72 eV, as well as IXs with lower energy of ~1.3–1.4 eV (figure S2). As we focus the laser spot on the PhC cavity (the area from where the holes are removed), a striking difference emerges in the PL response of the low energy spectrum: two narrow peaks are observed in the PL spectrum on the cavity, that are absent off of the cavity (see figure 2(A)). To measure the emission off the cavity, we focus our above-band laser away from the defect region, but still on the photonic crystal. The energies of these peaks are very close to the cavity resonances measured via transmission. By fitting the two narrow peaks in the PL, we found that the cavity Q-factor exhibited minimal degradation due to the heterobilayer transfer (see figure S3). By comparing the emission intensity on and off the cavity, we estimate the enhancement of the photon emission to be ~15 at the first resonance($\sim$ 1.37 eV).

To confirm the assignment of the low energy PL as originating from interlayer excitons, we performed PL excitation spectroscopy (PLE) on the heterobilayer region on the PhC cavity. Using a frequency tunable Ti:Sapphire cw laser (M^2 SolsTiS), we tuned the excitation energy across the excitonic manifolds of the isolated TMD monolayers (1.61 to 1.75 eV) while collecting the low energy PL. The PLE response, shown in figure 2(B), displays two broad resonances for the narrow peaks in the PL spectrum. Figure 2(C) presents the integrated PL spectrally degenerate with the cavity mode as a function of laser energy, which shows that the PLE resonances appear at the energetic positions of intralayer excitons in monolayer WSe_2 (1.72 eV) and monolayer $MoSe_2$ (1.64 eV). This result indicates that the PL comes from interlayer excitons [6, 9], which are excited through photon absorption in the monolayer WSe_2 ($MoSe_2$), followed by ultrafast interlayer charge transfer of the electron (hole), and subsequent formation of interlayer exciton, as illustrated in the insets of figure 2(C).

The polarization of the interlayer exciton PL on the cavity was then analyzed in the linear basis. The polarization-resolved PL measurements, shown in figure 3(A), reveal strong linear polarization of the narrow PL peaks. The integrated PL from the higher energy resonance (black arrows denote the integration region in figure 3(A)) is plotted as a function of the axis of linear polarization in figure 3(B). Comparison of the major axis of this linearly polarized PL with the orientation of the photonic crystal shows that it is directed along the $\hat{y}$ axis of the L3 cavity, which corresponds to a transverse electric polarized cavity mode, with only in-plane electric field components (see figure S4 in supplementary materials (stacks.iop.org/TDM/7/015027/mmedia)).

Under the electric dipole approximation, this implies that the optical coupling of the interlayer exciton has significant component in the plane of the heterobilayer, which is consistent with recent theoretical predictions [15, 16, 27, 28]. By scanning the objective lens, we also performed confocal spatial mapping of the polarization dependence of the PL across the entire PhC. The resulting spatial maps reveal a sharp peak in the intensity of $\hat{y}$-polarized interlayer exciton PL from the region on the cavity (I_y, figure 3(C)) that is absent from the spatial map of the $\hat{x}$-polarized interlayer exciton PL intensity (x, figure 3(D)). The spatial map of the cavity-enhanced PL defined herein as $I_{\mathrm{PhC}} \equiv I_{\hat{y}} - I_{\hat{x}}$, illustrates that it is spatially localized to the cavity (figure 3(E)). We note that there is another polarization-sensitive bright spot, which we attribute to the fabrication imperfections. New cavity designs

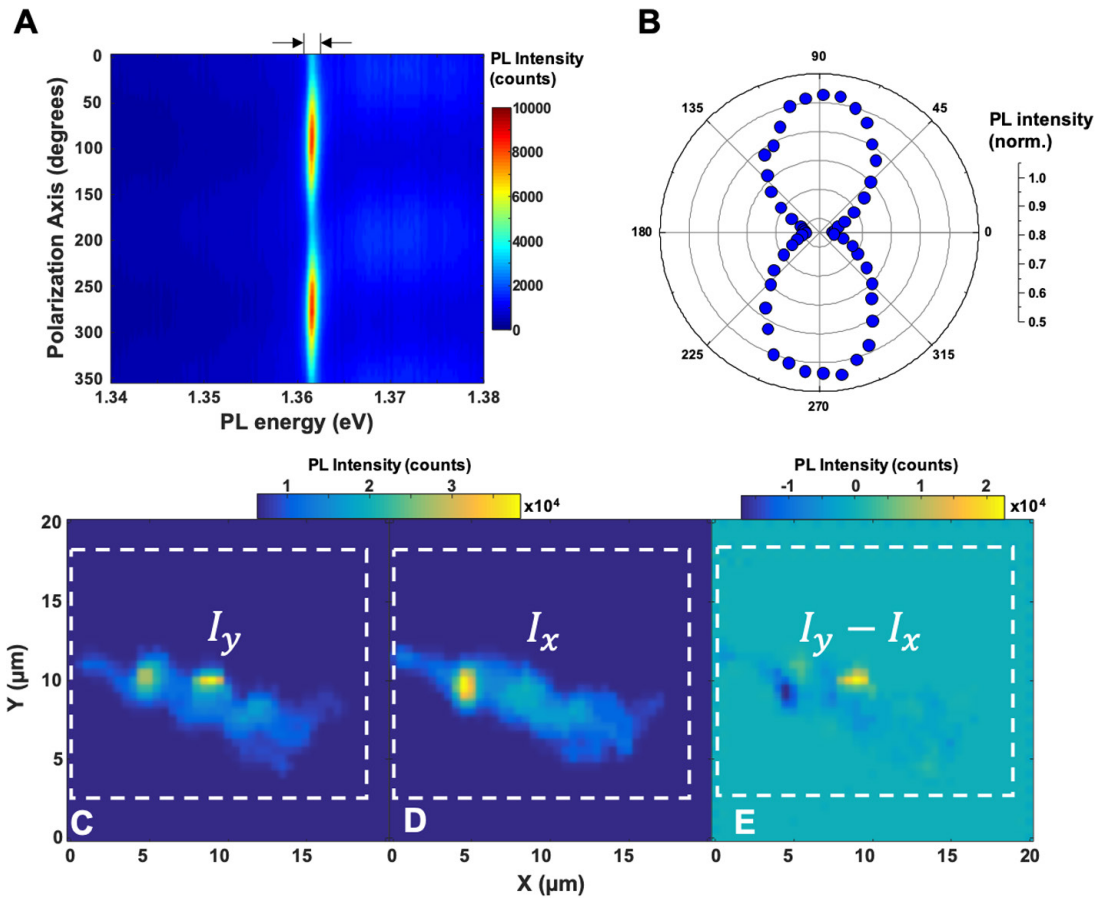

Figure 3. Polarization of cavity enhanced interlayer exciton photoluminescence. (A) Polarization-resolved photoluminescence (PL) from the interlayer exciton on the photonic crystal (PhC) cavity, in the linear basis. B Integrated PL intensity as a function of the axis of linear polarization. Integration region denoted by black arrows in (A). The major axis of the linear polarization is along the vertical direction ($\hat{y}$ axis in figure 1(D)). (C) and (E) Spatial maps of the integrated PL intensity from interlayer exciton with polarization directed along $\hat{y}$ (I_y, left) and $\hat{x}$ (I_x, center). Their difference ($I_y - I_x$, right) shows that the sharp PL peak is spatially located on the cavity of the PhC. The white dashed line shows the outline of the PhC structure.

supporting both transverse electric and transverse magnetic modes could provide more information on the in-plane and out-of-plane dipole of the interlayer exciton.

The dynamics of the cavity-enhanced PL were then characterized through time resolved PL measurements. A pulsed laser (1 MHz repetition rate, ~10 ps pulse duration) resonant with the A exciton of the WSe_2 monolayer (1.72 eV) was focused on the region of the heterobilayer on the cavity. The light is primarily collected from the bright spot in the spatial map of $I_{\hat{y}} - I_{\hat{x}}$ in figure 3(E). The polarization of the PL was analyzed along the $\hat{x}$ and $\hat{y}$ axes before being directed into a time-correlated single photon counting system. The narrow peak of cavity-enhanced PL was spectrally filtered to isolate the dynamic response of the PL resonant with the PhC cavity mode. The time-integrated cavity-enhanced PL under pulsed excitation is shown in figure 4(A). The dynamics of the PL resonant with the higher energy cavity mode (denoted by arrows on top of figure 4(A)) is shown in figure 4(B). We observe a significant difference in the decay of the interlayer exciton PL linearly polarized along the $\hat{x}$ and $\hat{y}$ axes of the PhC for the first ~200 ns, after which, the enhancement of the PL is diminished. The cavity-enhanced PL dynamics calculated via $I_{\hat{y}} - I_{\hat{x}}$ and shown in figure 4(C), are fit well by a triple exponential decay, with decay times of 1.3 ns, 20 ns, and 80 ns. Meanwhile, the PL after the first 200 ns is well fit by a double exponential with decay constants of about 116 and 670 ns. However, no appreciable lifetime reduction is observed in the exciton emission. We note that, as such, we do not have a clear explanation of the multi-exponential decays, and more studies are warranted.

Discussion

The obtained spectroscopic results support the coupling of the interlayer exciton in the $MoSe_2$–WSe_2 heterobilayer to the PhC L3 cavity. The energetic positions of the narrow peaks in the PL, 1.32 eV and 1.36 eV, closely match the energies of the bare photonic crystal cavity modes, measured at room temperature. Moreover, the narrow resonances measured in PL have similar quality factors as the bare cavities (measured via reflection, see figure S2), indicating low absorptive loss from the IX. The slight red-shift of the cavity modes with the heterobilayer on top is expected, as

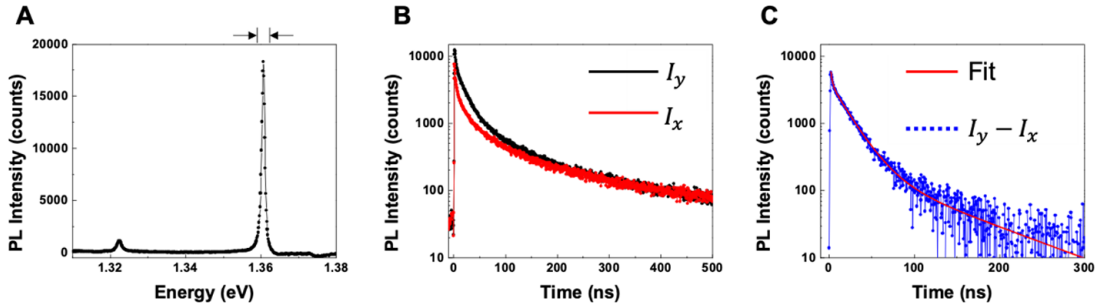

Figure 4. Dynamics of the cavity-coupled interlayer exciton photoluminescence. (A) Cavity-enhanced photoluminescence $(I_y - I_x)$ spectrum from the heterobilayer region coupled to the photonic crystal cavity. (B) Time resolved photoluminescence of the interlayer exciton photoluminescence with polarization along $\hat{y}$ (I_y, black) and $\hat{x}$ (I_x, red) directions. (C) Time-resolved cavity-enhanced PL ($I_y - I_x$, blue) with triple exponential fit (red).

the TMDs have higher refractive index than air. The PLE results clearly indicate that this PL stems from the interlayer exciton, rather than intralayer excitons confined in deep potentials. This assignment is further supported by the long decay dynamics of the PL, which are several orders of magnitude longer than ~ps lifetimes of intralayer excitons [29].

The total decay rate of the exciton population is given by the sum of the radiative and non-radiative recombination pathways, $\Gamma = \Gamma_{\text{rad}} + \Gamma_{\text{nrad}}$, and the cavity enhances only the radiative part. Hence, an emitter with large non-radiative decay rate ($\Gamma_{\text{nrad}} \gg \Gamma_{\text{rad}}$) cannot exhibit Purcell enhancement. The ground state of interlayer exciton has finite velocity, which implies vanishing oscillator strength. The interlayer exciton momentum relaxation therefore manifests itself as a fast non-radiative decay channel as the interlayer exciton transitions from a bright state to a dark state. Together with the large inhomogeneous broadening, this precludes conclusive determination of the lifetime reduction in this system (see supplementary discussion), although the enhancement of the PL intensity is evident. This enhancement of the PL intensity can originate from two effects: enhancement of the spontaneous emission rate and the cavity antenna effect. In most cavity quantum electrodynamic (cQED) systems involving solid-state emitters, the emitter is embedded inside the semiconductor, and thus already confined in the slab via total internal reflection. A cavity can redistribute the momentum vectors of the emission and provide better collection. In our system, however, the emitters are located on top of the semiconductor slab, and numerical simulation shows that the integration with the cavity reduces the collection efficiency: only ~8% of the light emitted from the heterobilayer on the cavity is collected by the objective lens, whereas we expect to collect almost ~32% of the light emitted from a heterobilayer placed on an unpatterned semiconducting substrate. This implies the radiative rate is actually enhanced by ~60 times (see supplementary discussion).

We can calculate the Purcell factor theoretically to be ~65, with a Q of 1370, mode volume of $\sim 0.7\left(\frac{\lambda}{n}\right)^3$, and emitter's position at the cavity surface $\left(\frac{E^2_{\text{surface}}}{E^2_{\text{center}}} = 0.44\right)$. We emphasize that, if a cQED system operates in the 'good cavity' regime, i.e. the cavity has smaller linewidth compared to the emitter, the Q used in calculation of the Purcell factor should be the Q of the emitter [30, 31]. However, our experimental results indicate that the cQED system is actually operating under the 'bad cavity' regime, which implies the homogeneous radiative linewidth of the emitter is narrower than the cavity, and the Q used in the Purcell factor calculation is that of the cavity. Our results laid a solid foundation in exploring more cQED effects in the nano-cavity integrated 2D heterostructure photonics.

Methods

Cavity fabrication

The cavity was fabricated from a 125 nm thick GaP membrane, grown via molecular beam epitaxy, on 1 μm thick sacrificial $Al_{0.8}Ga_{0.2}P$ layer on a GaP wafer. The patterns were first defined in ZEP520A resist by electron-beam lithography (JEOL JBX-6300FS, 100 keV) and then transferred to the GaP membrane by Argon and chlorine-based reactive ion etch. Excess resist was removed with dichloromethane. The sacrificial layer was undercut with hydrofluoric acid to yield suspended membrane structures with high index contrast, followed by cleaning in dilute KOH to remove any by-products of the undercut. The photonic crystal used in the experiment has a periodicity of $a = 264$ nm and radius of $r = 65$ nm. The cavity is created by removing three holes from a line, which is why the cavity is called linear three-hole (L3) defect cavity. The holes at the end of the cavity are shifted by $0.176a$, and the radius of those two holes are changed to $0.9r$, to increase the quality factor. These geometric parameters of the cavity are optimized via

finite difference time domain (FDTD) simulations using Lumerical FDTD solutions.

Photoluminescence spectroscopy

For PL measurements, a diode-pumped solid-state laser was used to excite the sample at 532 nm. The PL from the sample was collected in reflection geometry, normal to the plane of the heterobilayer and photonic crystal, using a 40× objective lens (0.6 NA). Cryogenic measurements were performed in a Montana Instruments Cryostation, in vacuum. The PL was dispersed by a 0.5 m monochromator equipped with a 600 line mm^{-1} groove density diffraction grating and a thermoelectrically cooled charge-coupled device (Andor Shamrock + Newton CCD) for time-integrated measurements. Polarization specific detection was accomplished by a combination of achromatic $\lambda/2$ waveplates and a linear polarizer. For PLE measurements, the excitation source was a power stabilized, frequency tunable cw Ti:Sapphire laser (M^2 SolsTiS). For time-resolved measurements, the excitation source was spectrally filtered output (~3 nm FWHM) from a supercontinuum laser with ~6 ps pulse duration and 1 MHz repetition rate. The PL was spectrally filtered (~2 nm FWHM) using a slit assembly mounted at the side port output of the monochromator before being directed onto a single-photon detector (Excelitas SPCM) connected to a time-correlated counting system (PicoHarp 300), with an overall instrument response time of ~450 ps. In all PL measurements, the excitation beam was spectrally filtered from the signal using a combination of dichroic beam splitters and long-pass filters.

Acknowledgments

This work is supported by the National Science Foundation under Grant NSF-EFRI-1433496, NSF MRSEC 1719797, NSF-ECCS-1708579 and the Air Force Office of Scientific Research Grant FA9550-18-1-0104. Part of this work was conducted at the Washington Nanofabrication Facility / Molecular Analysis Facility, a National Nanotechnology Coordinated Infrastructure (NNCI) site at the University of Washington, which is supported in part by funds from the National Science Foundation (awards NNCI-1542101, 1337840 and 0335765), the National Institutes of Health, the Molecular Engineering and Sciences Institute, the Clean Energy Institute, the Washington Research Foundation, the M J Murdock Charitable Trust, Altatech, ClassOne Technology, GCE Market, Google and SPTS.

Author contribution

XX and AM conceived the project. TKF fabricated and characterized the photonic crystal cavity. ER fabricated the heterobilayer and transferred it to the photonic crystal cavity, assisted by PR. PR performed spectroscopic the measurements, assisted by CL. YY performed the electromagnetic simulations of the far-field of the cavity. PR, AM, XX and WY analyzed the data. JY and DGM provided and characterized the bulk $MoSe_2$ and WSe_2 crystals. FH provided and characterized GaP. PR, AM, and XX wrote the paper. All authors discussed the results.

ORCID iDs

Pasqual Rivera https://orcid.org/0000-0002-5909-1686
Arka Majumdar https://orcid.org/0000-0003-0917-590X

References

[1] Geim A K and Grigorieva I V 2013 Van der Waals heterostructures *Nature* **499** 419–25
[2] Novoselov K S, Mishchenko A, Carvalho A and Castro Neto A H 2016 2D materials and van der Waals heterostructures *Science* **353** aac9439
[3] Rivera P *et al* 2018 Interlayer valley excitons in heterobilayers of transition metal dichalcogenides *Nat. Nanotechnol.* **13** 1004–15
[4] Lee C H *et al* 2014 Atomically thin p-n junctions with van der Waals heterointerfaces *Nat. Nanotechnol.* **9** 676–81
[5] Cheng R *et al* 2014 Electroluminescence and photocurrent generation from atomically sharp WSe_2/MoS_2 heterojunction p-n diodes *Nano Lett.* **14** 5590–7
[6] Rivera P *et al* 2015 Observation of long-lived interlayer excitons in monolayer $MoSe_2$–WSe_2 heterostructures *Nat. Commun.* **6** 6242
[7] Ceballos F, Bellus M Z, Chiu H Y and Zhao H 2014 Ultrafast charge separation and indirect exciton formation in a MoS_2–$MoSe_2$ van der Waals heterostructure *ACS Nano* **8** 12717–24
[8] Schaibley J R *et al* 2016 Valleytronics in 2D materials *Nat. Rev. Mater.* **1** 16055
[9] Nagler P *et al* 2017 Interlayer exciton dynamics in a dichalcogenide monolayer heterostructure *2D Mater.* **4** 025112
[10] Rivera P *et al* 2016 Valley-polarized exciton dynamics in a 2D semiconductor heterostructure *Science* **351** 688–91
[11] Jiang C *et al* 2018 Microsecond dark-exciton valley polarization memory in two-dimensional heterostructures *Nat. Commun.* **9** 753
[12] Miller B *et al* 2017 Long-lived direct and indirect interlayer excitons in van der Waals heterostructures *Nano Lett.* **17** 5229–37
[13] Jauregui L J *et al* 2018 Electrical control of interlayer exciton dynamics in atomically thin heterostructures *Science* **366** 870–5
[14] Unuchek D *et al* 2018 Room-temperature electrical control of exciton flux in a van der Waals heterostructure *Nature* **560** 340–4
[15] Yu H, Wang Y, Tong Q, Xu X and Yao W 2015 Anomalous light cones and valley optical selection rules of interlayer excitons in twisted heterobilayers *Phys. Rev. Lett.* **115** 187002
[16] Wu F, Lovorn T and MacDonald A H 2018 Theory of optical absorption by interlayer excitons in transition metal dichalcogenide heterobilayers *Phys. Rev.* B **97** (https://doi.org/10.1103/PhysRevB.97.035306)
[17] Ross J S *et al* 2017 Interlayer exciton optoelectronics in a 2D heterostructure p-n junction *Nano Lett.* **17** 638–43
[18] Dufferwiel S *et al* 2017 Valley-addressable polaritons in atomically thin semiconductors *Nat. Photon.* **11** 497–501
[19] Sun Z *et al* 2017 Optical control of room-temperature valley polaritons *Nat. Photon.* **11** 491–6
[20] Liu C H *et al* 2017 Nanocavity integrated van der Waals heterostructure light-emitting tunneling diode *Nano Lett.* **17** 200–5
[21] Fryett T K *et al* 2016 Silicon photonic crystal cavity enhanced second-harmonic generation from monolayer WSe_2 *2D Mater.* **4** 015031

[22] Day J K, Chung M-H, Lee Y-H and Menon V M 2016 Microcavity enhanced second harmonic generation in 2D MoS_2 *Opt. Mater. Express* **6** 2360
[23] Gan X T *et al* 2018 Microwatts continuous-wave pumped second harmonic generation in few- and mono-layer GaSe *Light Sci. Appl.* **7** 17126
[24] Wu S *et al* 2014 Control of two-dimensional excitonic light emission via photonic crystal *2D Mater.* **1** 011001
[25] Englund D *et al* 2010 Resonant excitation of a quantum dot strongly coupled to a photonic crystal nanocavity *Phys. Rev. Lett.* **104** 073904
[26] Zomer P J, Guimarães M H D, Brant J C, Tombros N and van Wees B J 2014 Fast pick up technique for high quality heterostructures of bilayer graphene and hexagonal boron nitride *Appl. Phys. Lett.* **105** 013101
[27] Yu H, Liu G-B and Yao W 2018 Brightened spin-triplet interlayer excitons and optical selection rules in van der Waals heterobilayers *2D Mater.* **5** 035021
[28] Lin Y-C *et al* 2015 Atomically thin resonant tunnel diodes built from synthetic van der Waals heterostructures *Nat. Commun.* **6** 7311
[29] Palummo M, Bernardi M and Grossman J C 2015 Exciton radiative lifetimes in two-dimensional transition metal dichalcogenides *Nano Lett.* **15** 2794–800
[30] Javerzac-Galy C *et al* 2018 Excitonic emission of monolayer semiconductors near-field coupled to high-*Q* microresonators *Nano Lett.* **18** 3138–46
[31] Chen Y *et al* 2018 Deterministic positioning of colloidal quantum dots on silicon nitride nanobeam cavities *Nano Lett.* **18** 6404–10